CHAPTER 4

EXPERIMENTAL RESULTS AND DISCUSSION

4.1 Initial Microstructure Characteristic

Using optical microscope, it was found that the microstructure consisted of polycrystals of a uniform equiaxed grain characteristic. The mean diameter ($d_{m)}$ of the Ni-matrix grain size was 0.065 mm approximately. There were coarse block-like MC carbides precipitating within grains and also grain boundaries resulting from eutectic reaction [7]. The morphology of these carbides is shown in Figure 4.1. These coarse carbide particles in matrix were arranged in chain-like formation resulted from previous rolling process. The effect of MC coarse carbide to mechanical properties is due to local stress or high stress concentration around coarse carbides. The local stress resulted from the difference of modulus produced in coarse carbides and austenite matrix phase. In addition to local stress, the difference of thermal expansion between in coarse carbides and matrix phase also involved in the change of mechanical properties especially in high temperature testing. This local stress and thermal expansion affected to the behaviour of fracture process. Therefore, cracks would originate at these coarse carbides.

It is also possible to see the fine carbides in the as-polish condition located in grain boundaries of the specimen as shown in Figure 4.2. This fine carbide phase along grain boundries have beneficial role for preventing the occurrence of the grain

boundry sliding. Using EDX analysis, these carbides are complex carbide which was in $M_{23}C_6$ carbides class [7]. Annealing twins as result from heat treatments were observed in etched specimens, as shown in Figure 4.3.

The TEM microstructures as shown in Figure 4.4 and 4.5 illustrated that the spherical morphology of gamma prime particles is uniformly distributed. This morphology was produced by two steps heat treatment of precipitation aging [7]. The gamma prime particles in matrix had estimated diameter of 50-80 nm. No size heterogenity was observed. The gamma prime phase is intermetallic Ni_3 (Al,Ti) phase with face centered cubic (FCC) structure [7]. The gamma prime were full coherency with austenite matrix. It was found that gamma prime acted as a barrier for preventing the movement of dislocation passing the gamma prime particles either by Orowan bowing or cutting (shearing) mechanism. The ability for hinding dislocation also depends on their chemical compositions.

Furthermore, with thermal activation, the movement of dislocation which passing the particles may be occurred by another mechanism involving an increase of temperature i.e., climbing in long term testing.

4.2 Tensile Property

The results of tensile tests at ambient temperature (T=25°C) are summarized in Table 4.1. The test data were obtained and compared with the specification of the

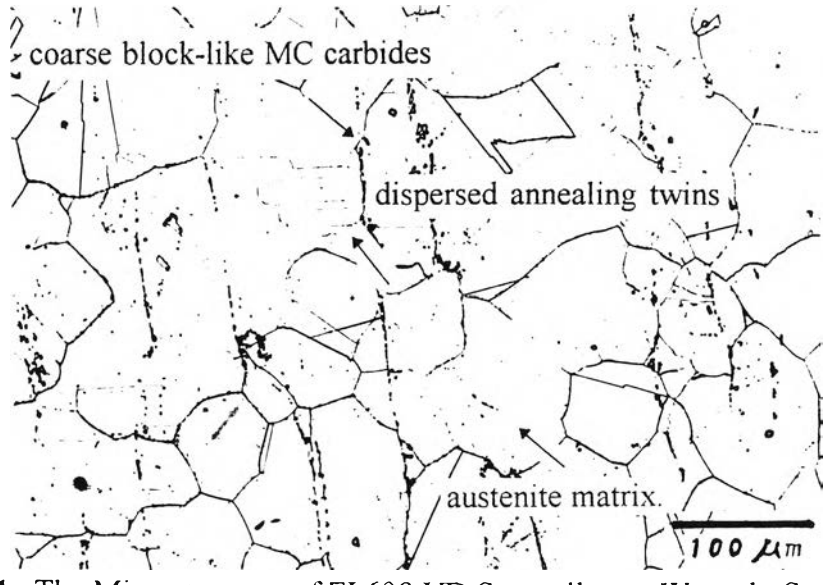

Figure 4.1 The Microstructure of EI 698 VD Superalloy as Wrought Structure (as polished) 50 X

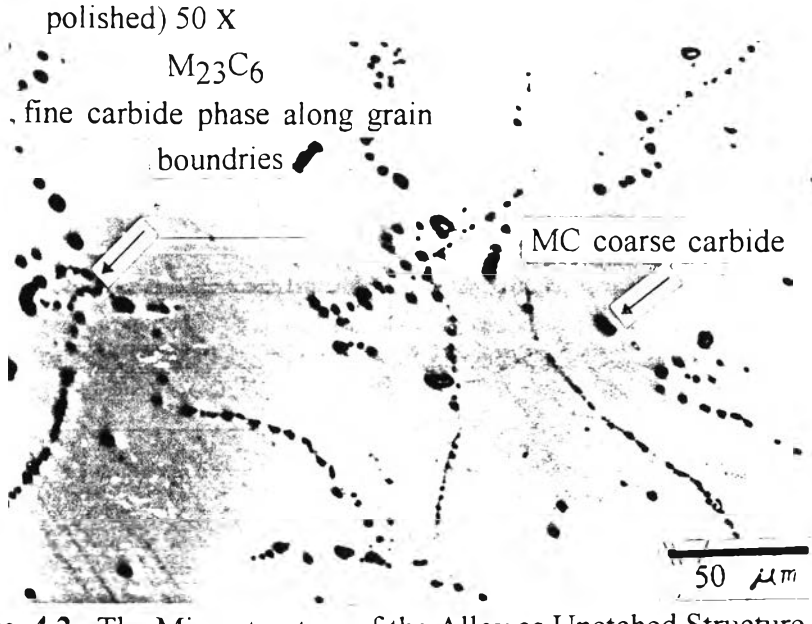

Figure 4.2 The Microstructure of the Alloy as Unetched Structure 100 X

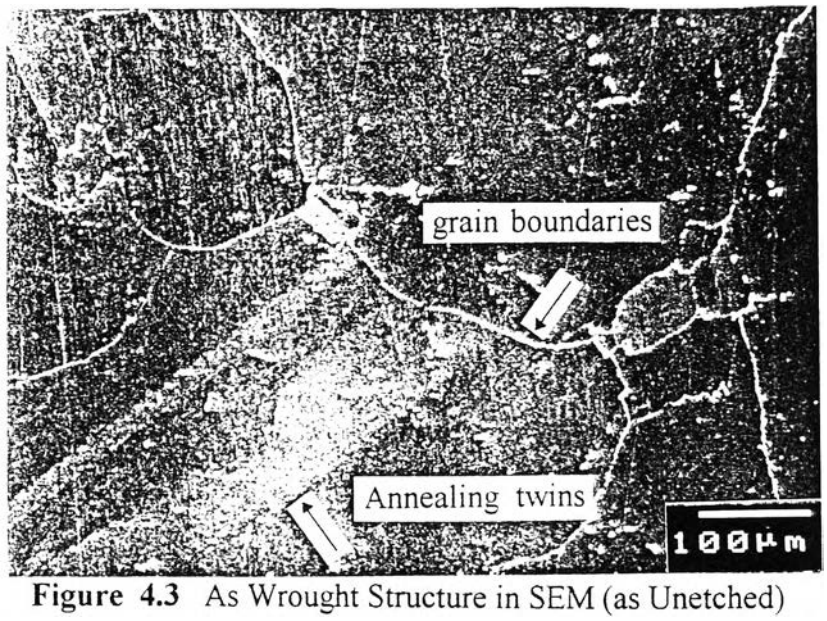

Figure 4.3 As Wrought Structure in SEM (as Unetched)

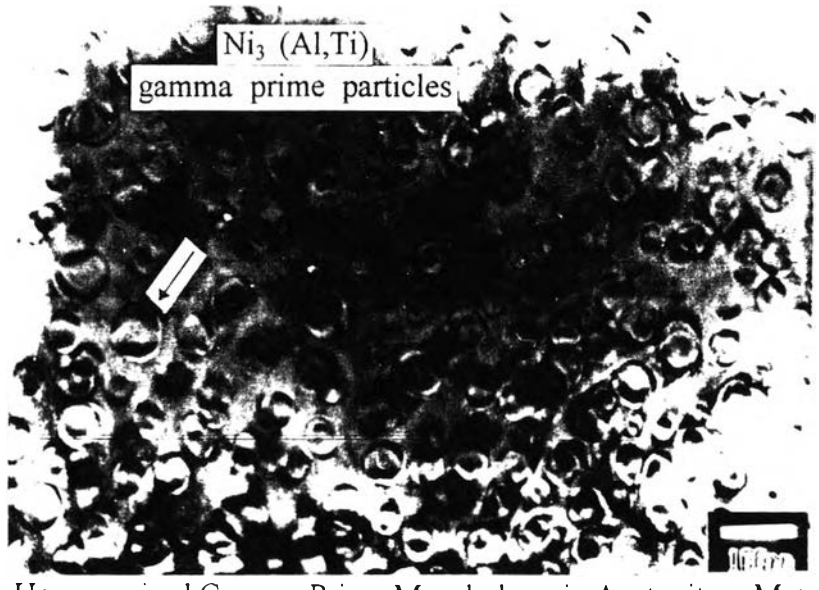

Figure 4.4 Homogenised Gamma Prime Morphology in Austenite mMatrix in TEM

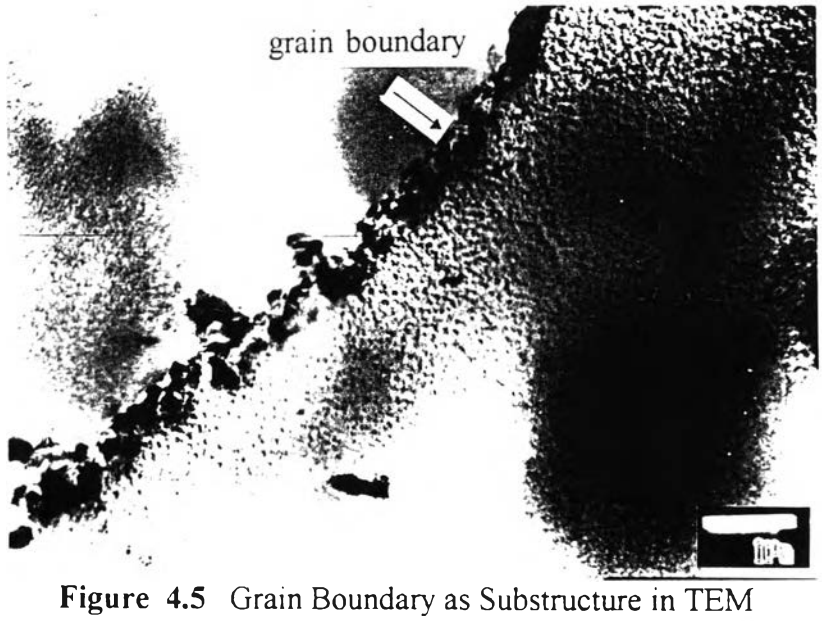

Figure 4.5 Grain Boundary as Substructure in TEM

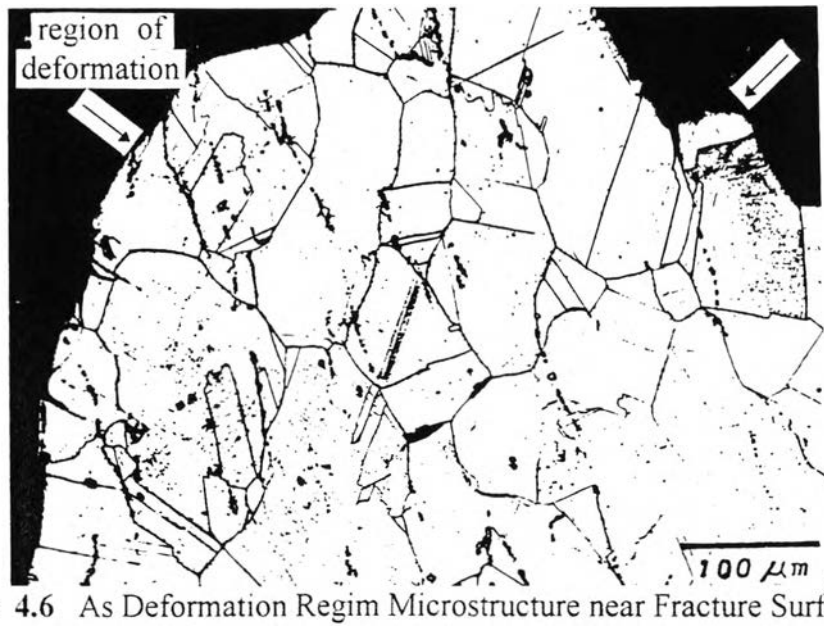

Figure 4.6 As Deformation Regim Microstructure near Fracture Surface 50 X

alloy prescribed by the Russian aviation testing standard TU-73[7]. This obtained data showed that these tensile results were in agreement to the standard for rupture and yield strengths. The results of tensile tests at elevated temperature (T =650°C) are also given in Table 4.1.

Tested Temperature (°C)	Yield Stress (MPa)	Average Yield Stress (MPa)	Rupture Stress (MPa)	Average Rupture Stress (MPa)
25°C / Test.1	792	780.5	1,175	1,160.5
25°C / Test.2	769		1,146	
650°C / Test.1	688	680	1,016	1,028
650°C / Test.2	672		1,040	

Table 4.1 Tensile Properties at Room and Elevated Temperatures tests

The results from both tables above imply that temperature was the important factor on mechanical properties of the alloy. At elevated temperature tests, It was found that the yield strength and strength at rupture point were lower than those in ambient temperature. Certainly the increase on ductility and reduction of area were observed due to increase in plastic deformation. These phenomenon were in the same

manner as found by many previous works **[1,5,15,16,17,18].** These tensile properties of the alloy might occur from these following effects **[5]**:

1. High temperature will result in the greater mobility of dislocation by the mechanism of climb and the higher equilibium concentration of vacancies with increasing temperature.

2. Slip system changes, or additional slip systems are introduced with increasing temperature.

3. Higher deformation at grain boundaries occured when the temperature of metals increased.

The main aim of these tensile tests was just to recieve the values of mechanical properties, under tensile at room and elevated temperature conditions, for yield and maximum tensile strength for further using in maximum stress consideration for creep, isothermal cyclic creep and cyclic creep with thermomechanical fatigue.

4.3 Microstructure Analysis of All Tested Specimens

The in microstructure of tested specimens under different creep stress levels (612, 706, 740, 760 and 850 MPa), isothermal cyclic creep and cyclic creep with TMF, were investigated by optical microscope and showed no significant change in characteristic. The all results showed that high temperature deformation from three above testing conditions caused very negligible changes of shape and size of austenite

grains. Only the regime close to fracture surface, individual grains were observed with visible deformation. The calculated strains (elongation) less than 10 % observed in all tests, did not produce the very high in grain elongation regardless to the applied stress levels. However, the large region of deformation was near fracture surface occuring from stress concentration, as shown in Figure 4.6. There was observation that dispersed annealing twins in the matrix were still existing.

Distribution of coarser block-like MC carbides precipitation were found in chain form. These coarse carbides were very often fracture as shown in Figure 4.7. Cracks appeared to be perpendicularly propagating toward applied loading direction as an effect of difference in modulus of elasticity between coarser block-like MC carbide and matrix. In case of cyclic creep with TMF, this type of crack may include additionally the effect of difference of modulus of elasticity between matrix and carbides and/or physical properties (thermal expansion and thermal conductivity).

However, in all specimens, there were found few small crack openings along grain boundaries located either on the specimens surface or in interior of specimens as shown in Figures 4.8 a and b. These small cracks should occur from decohesion of grain boundary continuing to generate continuous linking of cavities in grain boundaries and/or grain boundary sliding. Then surface cracks and interior specimen cracks always initiated on grain boundaries. These surface cracks and interior specimen cracks were dominantly nucleated and grew along grain boundaries oriented perpendicularly toward to the applying loading (longitudinal specimen axis).

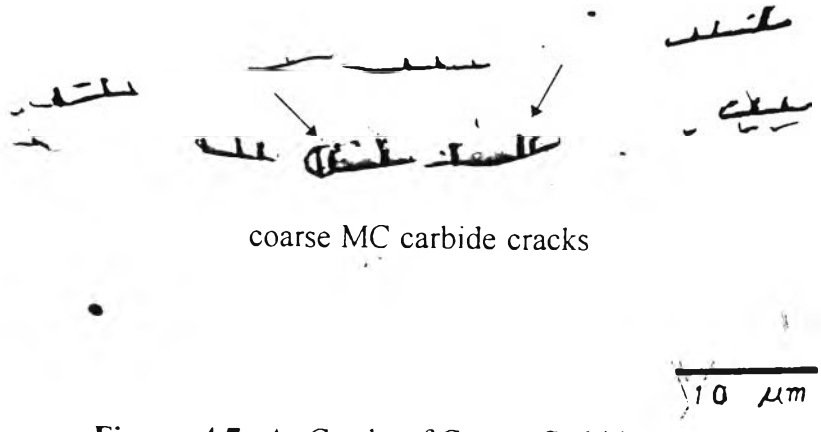

Figure 4.7 As Cracks of Coarse Carbides 500 X

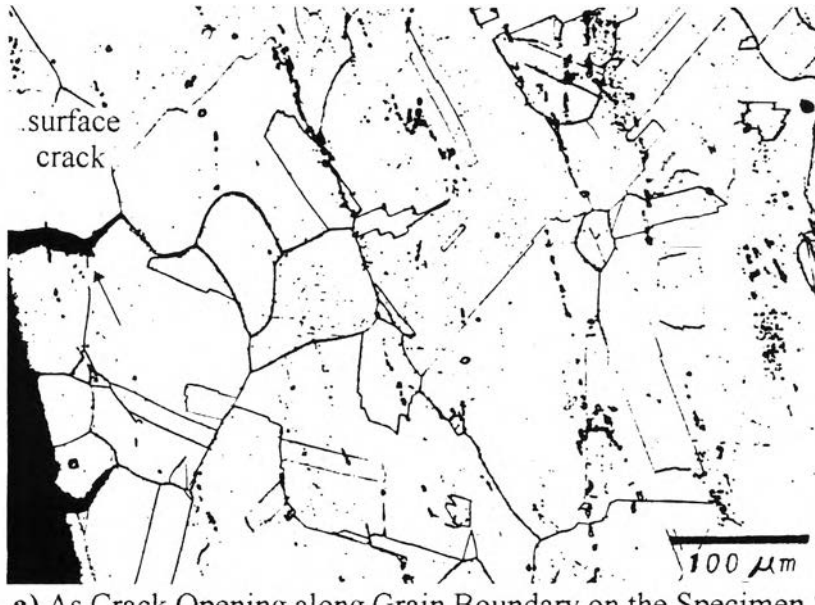

Figure 4.8 a) As Crack Opening along Grain Boundary on the Specimen Surface 50 X

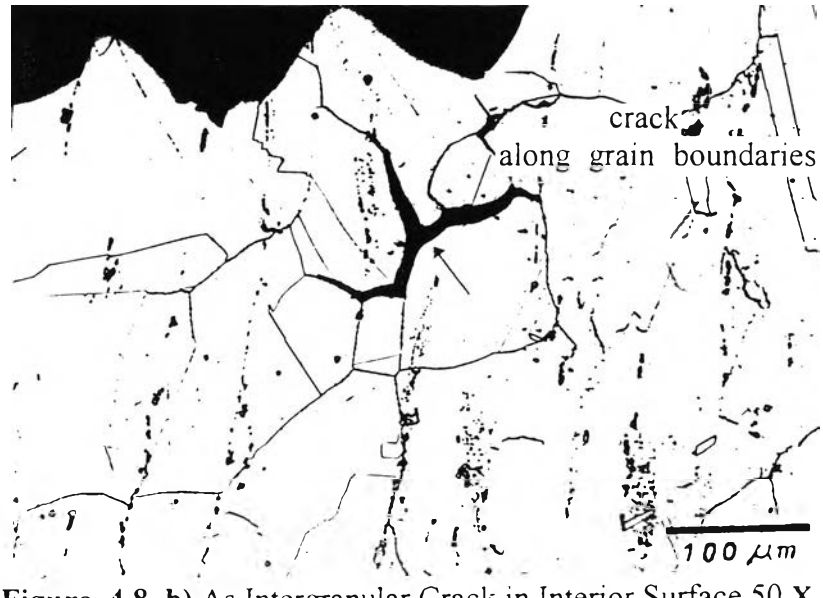

Figure 4.8 b) As Intergranular Crack in Interior Surface 50 X

There were also frequent observations in gauge length region showing that the blocky carbide particles were weak point of structure which would affect to fracture mechanism. At coarser MC carbides, the cracks were also in perpendicular position to acting stress in the matrix. The destructive process also included the formation of cavities on interface between matrix and carbide surface. However, it was found in the area where was far from fracture surface that this type of coarse MC carbide cracks never propagated through grain leading to generate transgranular cracks. Therefore, these coarse MC carbide cracks were not aspected for major affecting to final fracture mechanism. This evidence can also confirmly indicate that there was very small grain deformation occuring in area far from fracture surface.

Few features of deformation in grains or slip bands were observed occuring near fracture surface, as shown in Figure 4.9. Fracture profile line confirmed that the dominant propagation of main crack was along grain boundaries, as shown in Figure 4.10. For unfractured crept specimens which were carried out at stress R = 740 MPa. and temperature T = 650°C for 1 hour-transient creep and 25 hours-steady state creep, no changes in microstructure were observed due to very low deformation (low stain), as shown in Figure 4.11.

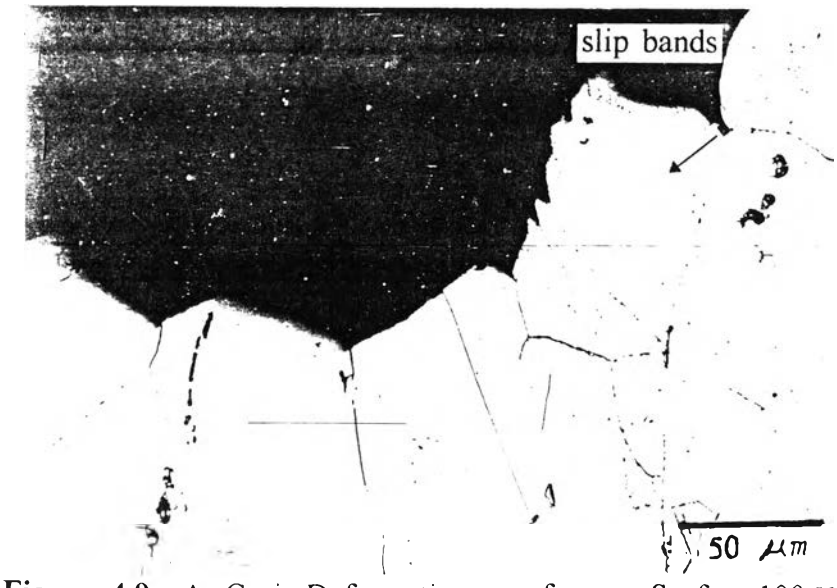

Figure 4.9 As Grain Deformation near fracture Surface 100 X

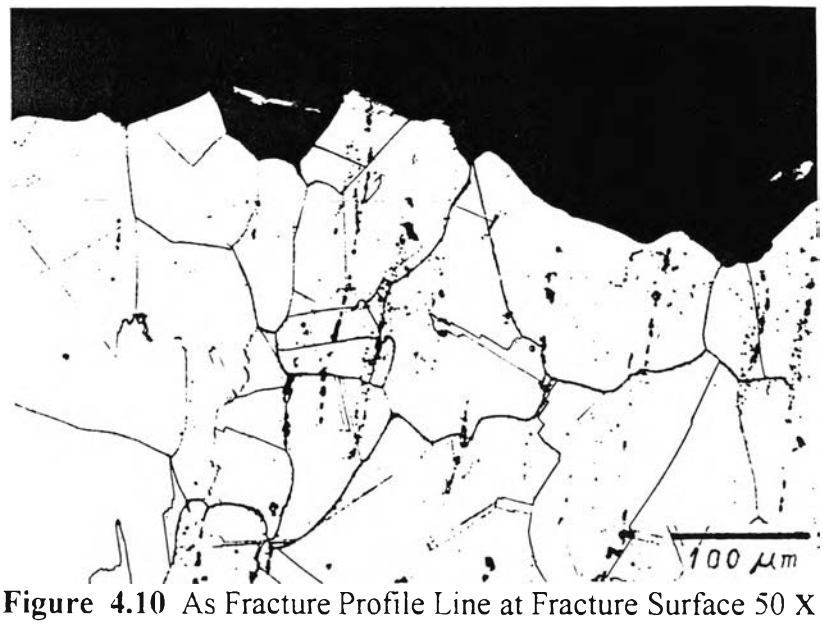

Figure 4.10 As Fracture Profile Line at Fracture Surface 50 X

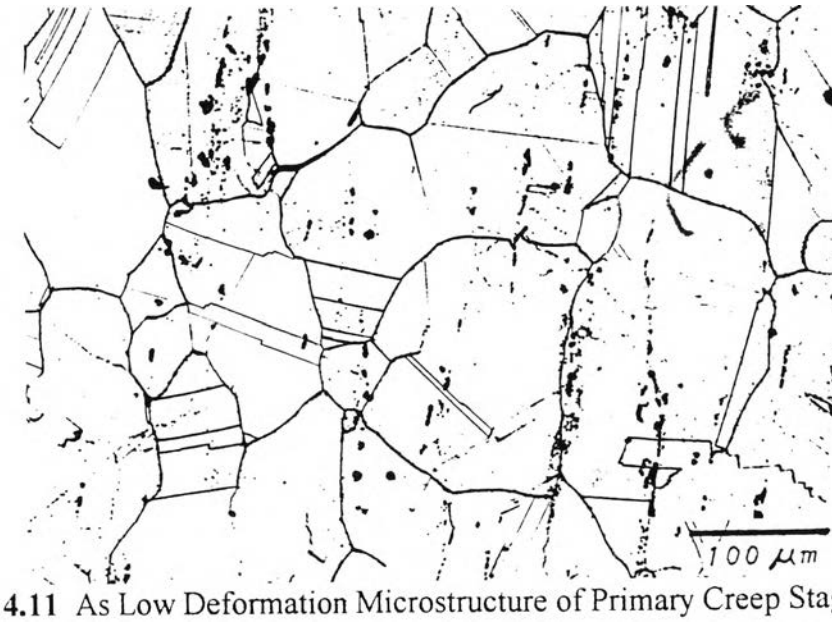

Figure 4.11 As Low Deformation Microstructure of Primary Creep Stage 50 X

4.4.1 Substructure Analysis of Crept Specimens

In case of pure creep, the specimens from creep deformation process of the alloy for three creep stages, at only defined stress level (740 MPa.) and temperature (650°C) testing condition, were analysed using TEM of thin foils. This test was aimed to reveal substructure development due to dislocation movement in the individual stage of primary, secondary and tertiary creep. The visible substructure changes were observed as result of interaction between dislocation and gamma prime precipitated particles. In all analysed specimens, gamma prime particles were still unimodal size and distribution. Thus this observation implies that during the creep deformation the shape and size of gamma prime phase were not affected extensively by diffusional creep process which was dominate in low creep rate tests **[6]**.

In primary or transient creep stage, the specimen was cut after 1 hr. test. The ununiform distribution of dispersed gliding dislocations was observed in each of the individual grain, Figure 4.12. These dislocations concentrated partially in some regims of the matrix and hereby generated dense dislocation networks formation. The major mechanism concerning with the movement of dislocation passing the precipitates was Orowan bowing mechanism where presented in the regims among individual wide slip bands, Figure 4.13. Very low amount of dislocation loops as a result of Orowan bowing were also observed in the location around the particle-matrix interface, Figure 4.14. The another mechanism of deformation i.e., dislocations shearing the gamma prime particles causing narrow stacking faults formation inside of

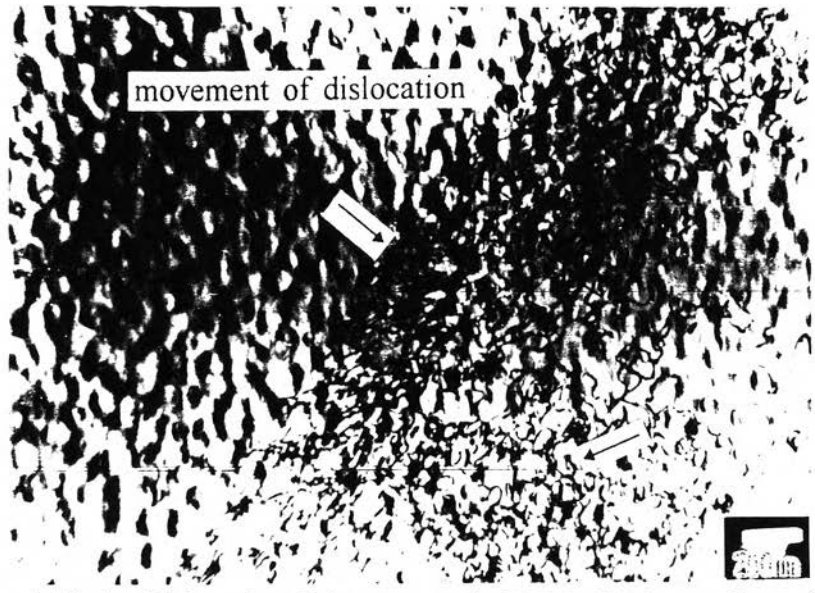

Figure 4.12 As Dislocation Substructure in TEM of Primary Creep Stage

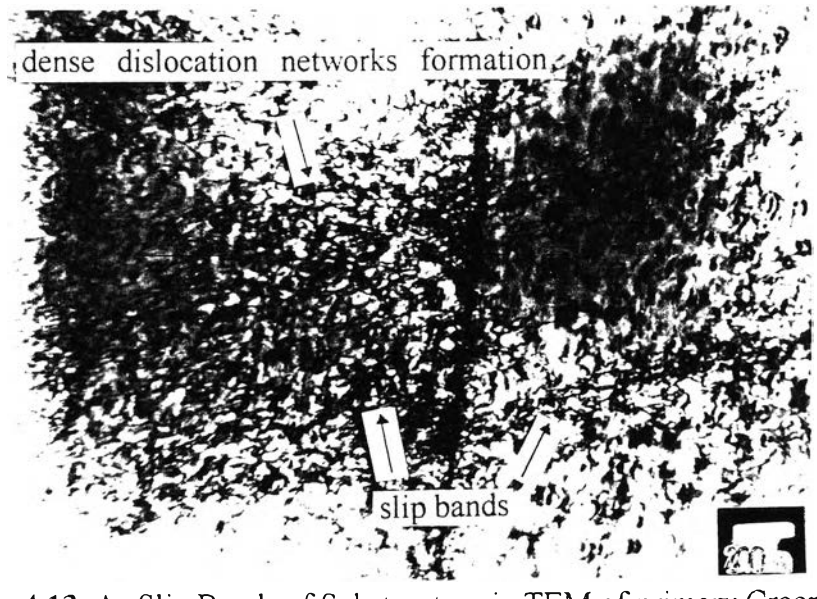

Figure 4.13 As Slip Bands of Substructure in TEM of primary Creep Stage

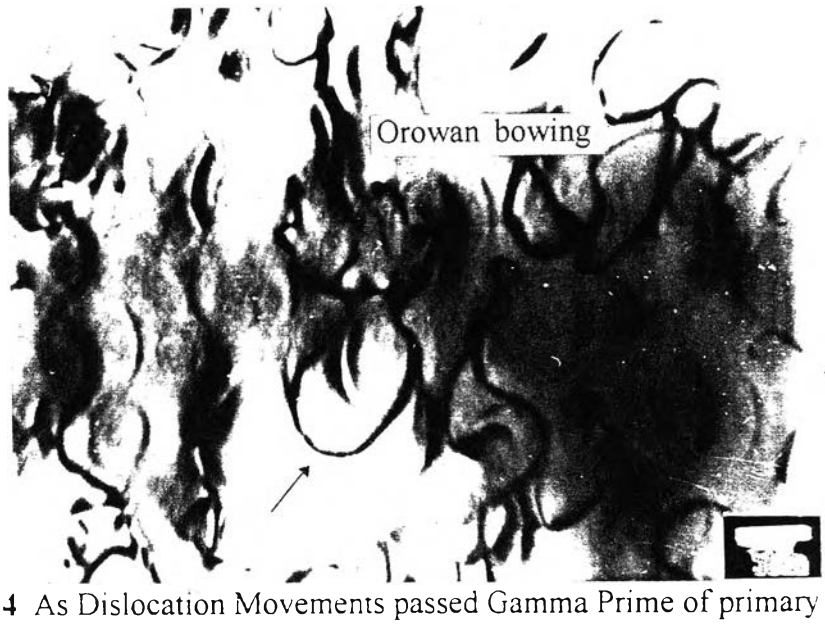

Figure 4.14 As Dislocation Movements passed Gamma Prime of primary Creep Stage in TEM

the entire particles, Figure 4.15. The dislocation shearing of precipitate particle could occur because of the extensive work hardening within the slip bands **[13]**.

In secondary creep stage, the specimen was cut after 25 hrs. test. The dominant deformation mechanism was Orowan bowing. The dislocation networks were formed more dense and homogeneously distributed than in primary creep stage, Figure 4.16. The density of dislocation was also greater in the areas near grain boundaries due to dislocation pile up, Figure 4.17.

In tertiary creep stage, the specimen were analysed after fracture. The main observed dislocation mechanism was also Orowan bowing which was similar to secondary creep stage, Figure 4.18. The dislocation formation was networks distribution which was more dense and homogeneously than those of secondary creep stage. However, the existing of the shearing mechanism in TEM microstructure in secondary and tertiary creep stages was difficult to investigate difmitely or unclear. Thus in tertiary creep stage before, very dense dislocation networks formation as a result of dislocation pile up mechanism might provide work hardening and thus affected to reduction in ductility.

4.4.2 Mechanical Properties of Creep Deformation

The data and the results of creep tests were carried out at different stress levels and at constant elevated temperature T = 650°C as stated in Table 4.2. It could be seen that the stress level of creep tests carring out at 706, 740, 760, and 850 MPa. were

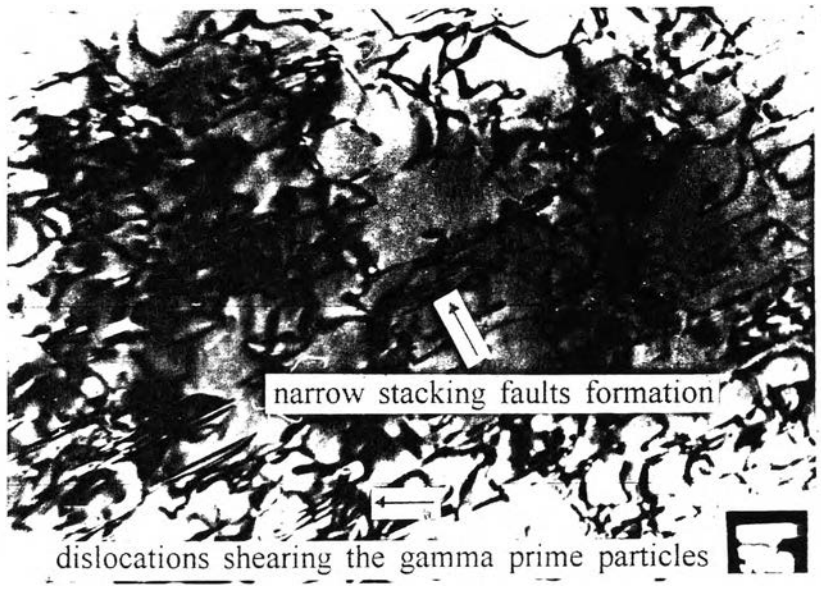

Figure 4.15 As Particles Shearing Mechanism of Substructure in TEM

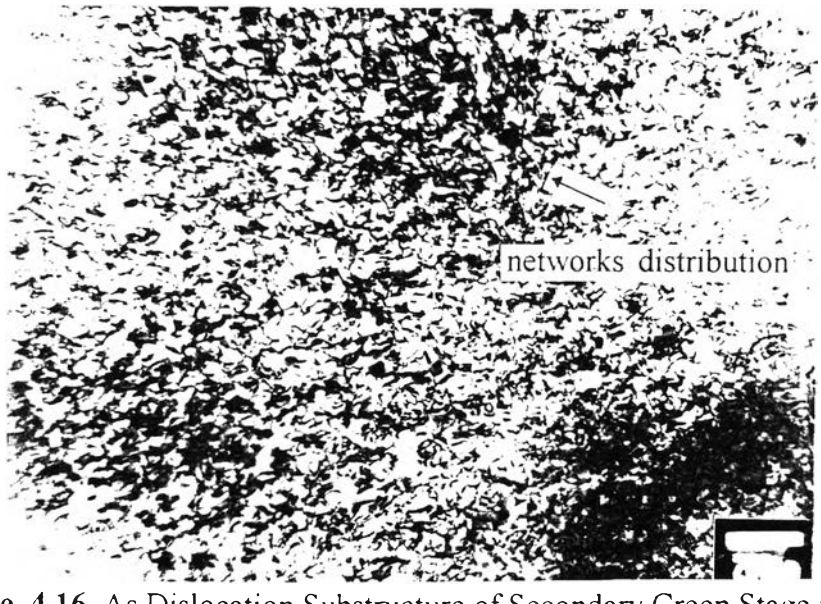

Figure 4.16 As Dislocation Substructure of Secondary Creep Stage in TEM

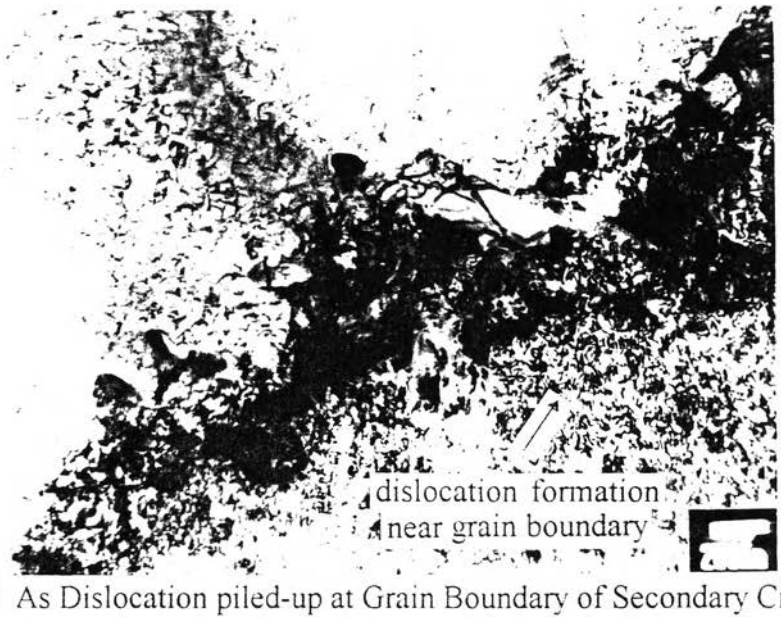

Figure 4.17 As Dislocation piled-up at Grain Boundary of Secondary Creep Stage Substructure in TEM

higher than the yield strength R = 680 MPa. (obtained from tensile test at elevated temperature T = 650°C). The only one creep test carring out at stress level R = 612 MPa which was below the obtained yield stress value. The results showed that creep fracture lifetimes inversely varied with stress levels. The lowest stress at R = 612 MPa produced the longest lifetime. On the other hand, the highest stress at R = 850 MPa. gave the shortest lifetime, as shown in Figure 4.19 and Table 4.2. This phenomenom is in agreement on many previous works on creep of materials **[3,5,6,7,16,17,18]**.

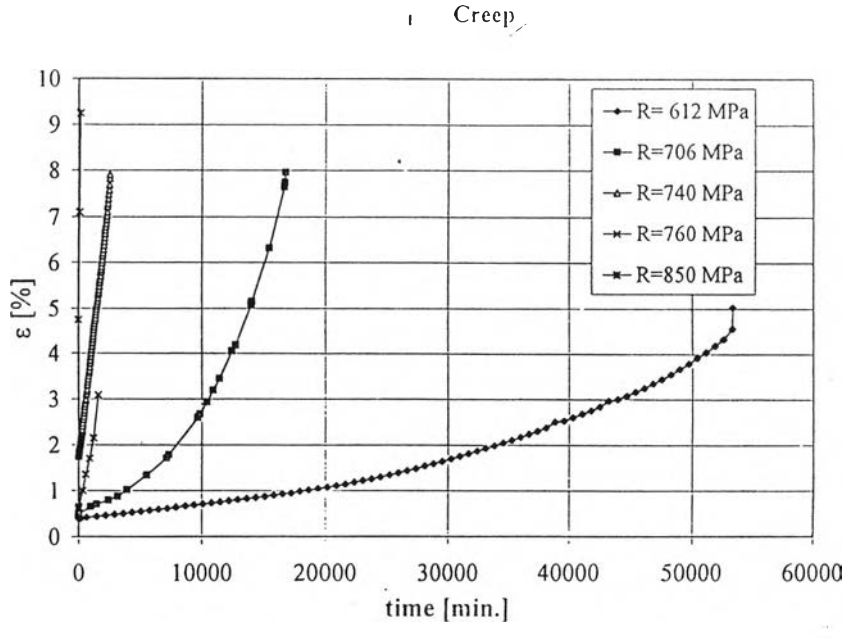

Diagram 4.1 Diagram of Strain-Time of Creep Tests

Stress Levels (MPa)	Fracture Strain (%)	Creep Life Time (min)	Strain Rate (mm/hr)
612	5.03	53,310	7.03×10^{-3}
706	7.96	16,800	1.2×10^{-3}
740	7.912	2,503	5.135×10^{-2}
760	3.1	1,560	1.4×10^{-2}
850	9.25	140	3×10^{-1}

Table 4.2 Creep Tests Properties

Another investigations was study of the relationship among stress level lifetime and maximum strain. The assumption is that the lower applied stresses (longer lifetime) would provide lower maximum strains. This fracture strain behaviour as an effect of stress levels were according with several previous works **[3,5,6,7]**. The initial strain instantly occured after loading depends upon the stress level and increased with increasing stress. The relation between steady-state creep rate and stress level, exhibited that higher stress levels produced higher secondary creep rate, as it can be seen in set of creep curves of Diagram 4.1. However, only creep test at stress level R = 760 MPa expressed the strain-time behaviour different fromthe other creep tests. This could be explained as probable effects of structure heterogenity, especially the size and distribution characteristics of coarse MC carbide particles in grains.

In Figure 4.19, it can be seen that the deformation of creep curves did not start at the same point since the effect of different applied stresses. This can be explained that for higher stress levels the greater stresses were obtained to deform the alloy more than those of lower stress levels as an effect of testing impact. Thus the deformation generated faster (strain rate) and higher (strain) than that in lower stress levels.

Only in creep test at high stress level at 740 MPa, there were carried out the microstructure observation by TEM at each creep stage for primary, secondary and tertiary creeps in each stress level test. Thus this could be identified that what creep mechanism development happened in each stage of the alloy under creep stress level at 740 MPa.

The TEM of thin foils was used to study the creep deformation corresponding to individual creep stage for creep carring out at 740 MPa stress level. For primary creep stage, there was evident to show that few planar slips occurred within the grains and very low amount of initial dislocation networks as a result of very low deformation, Figures 4.13 and 4.14. The major observed mechanism to overcome precipitates in this stage was by-passing the precipitates by Orowan bowing among individual slip bands. However, these Orowan bowings did not fully envelope precipitates. When work hardening increased by dislocations piling up, dislocations moved difficultly, and lead to a decrease in creep rate. Therefore the steady-state creep stage began. Another dislocation interaction, shearing precipitate particles in slip bands, would set up preferential paths for the movement of dislocation in early stage

of deformation **[17]**. In previous works **[3,5,6]** explained that the final of primary creep stage would be reached when there was balancing between work hardening and recovery processes occurring.

The previous research **[17]** reported that the secondary creep arose not only from the mechanism of grain boundary sliding and slips within the grains but more particularly from movement of dislocations within the grains. In present work, the TEM observation on secondary creep stage of creep stress level at 740 MPa illustrated in the same manner with above explanation. This tangling dislocation density in secondary creep stage was higher that of primary creep stage, Figure 4.16. Additionally, these dislocations movement within the grains such as Orowan bowing might be the interaction controlling the steady state creep rate.

In creep curves of creep stress levels at 612 and 740 MPa the strain increased from origin point and reached the end point of steady state creep stage, Diagram 4.1. The creep development exhibited by running point deviate from linearlity and obtained highly increasing in slope indicating for tertiary creep stage. This would occur by result of increasing in stress concentration due to change in the cross-section area, namely localized necking. Furthermore, the increase in creep strain resulted partly from the development of intergranular cavities as shown in Figure 4.19. Subsequently the initiation of crack would occur from an agglomeration of cavities along grain boundaries with the expense of decreasing in the intervoid spacing. Therefore voids can link up together leading to intergranular creep failure. However, from the another

Figure 4.18 As Dense Dislocation Substructure of Tertiary Creep Stage in TEM

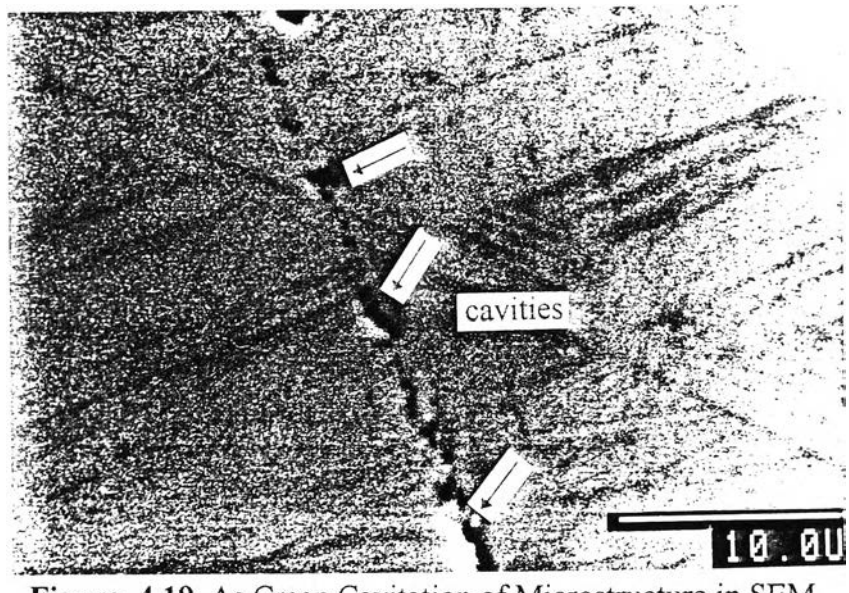

Figure 4.19 As Creep Cavitation of Microstructure in SEM

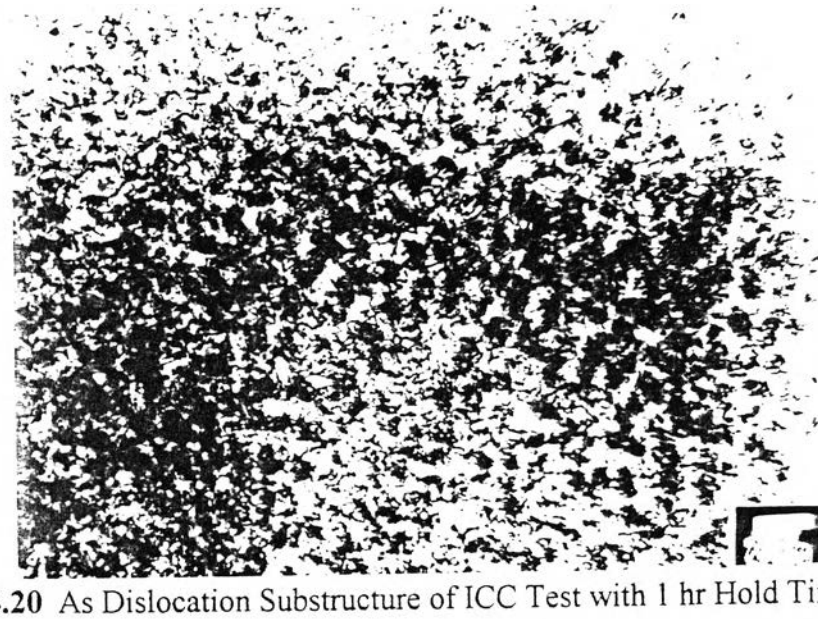

Figure 4.20 As Dislocation Substructure of ICC Test with 1 hr Hold Time in TEM

research [17] reported that intergranular cracks also occurred before the tertiary stage due to they were developed already at the end of secondary creep.

Nevertheless, the mechanism of fracture occurred in this present work was not only intergranular fracture, but mixing fracture mode between intergranular and transgranular also. This was discussed in details in the fractography section .

4.5.1 Substructure Analysis of Isothermal Cyclic Creep and Pure Fatigue Tests

The investigation on dislocation/precipitates interaction was performed on the isothermal cyclic creep tested specimens after rupture. The main aim was to investigate the effect of varying holding times introducing onto cyclic stress waveform. This holding time affected to dislocation development. The result of isothermal cyclic creep test with 10 hrs. holding time was revealed that the final microstructure after fracture consisted of very dense dislocation networks in matrix due to high deformation. The principal strengthening mechanism involving dislocation movements via precipitates was still Orowan bowing, as shown in Figure 4.20. Substructure characteristics were similar to those of crept specimen as mentioned in substructure analysis of creep tests section.

However, specimen under isothermal cyclic creep test with 1 hr. holding time condition revealed that particles shearing was major interaction as illustrated in Figure

4.21. As a result of dislocation shearing particles which set up preferential paths for the movement of dislocation in early stages of individual cyclic, the stacking faults formation throughout the particles were observed. Therefore, this dislocation shearing precipitate particle interaction might relate to deformation characteristics resulting in cyclic softening behaviour. For example, strain and strain rate were higher than those of other longer holding times of isothermal cyclic creep tests which were controlled mainly by dislocation bowing interaction. The dislocation networks were more dense near fracture surface and grain boundaries where corresponded to the high degree of deformation, as seen in Figure 4.22. Thus these very dense dislocation networks were generated with higher deformation in the similar manner of creep before fracture. The morphology of precipitate particles was still found in spherical shape.

In the case of pure fatigue at constant high temperature test, or in mean of no holding time, resulted in cyclic strengthening and very low elongation (1.25% approximately) of specimen as illustrated in Diagram 4.2. The dislocation analysis in specimen which was intercepted after 2,200 cycles, indicated that principal deformation was multiple slip bands in different slip plane directions, Figure 4.23. The dislocation tangles within these narrow bands and at the intersection of slip planes were very dense, Figure 4.24.

If further cycling lead to more dense dislocation tangles within multiple slip bands and/or caused the formation of other slip bands. The higher work hardening would be resulted when multiple slip was generated. This was due to the effect of slip

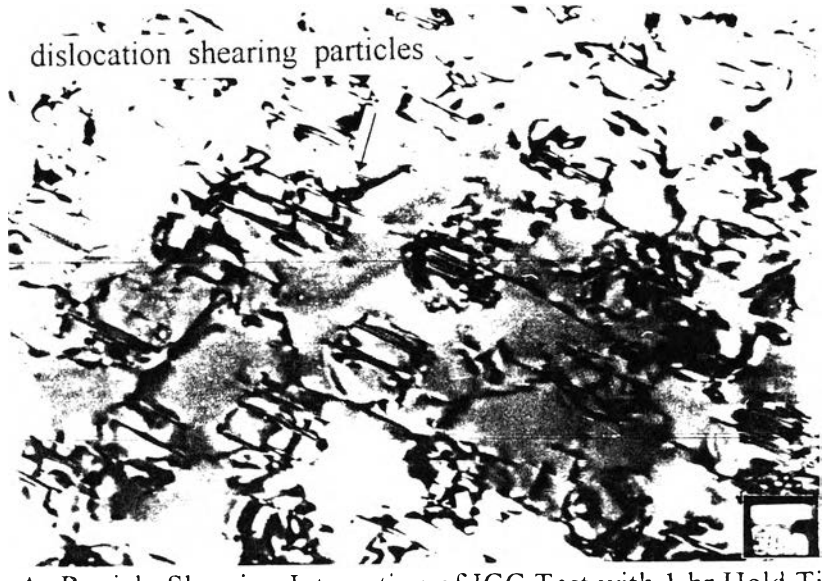

Figure 4.21 As Particle Shearing Interaction of ICC Test with 1 hr Hold Time in TEM

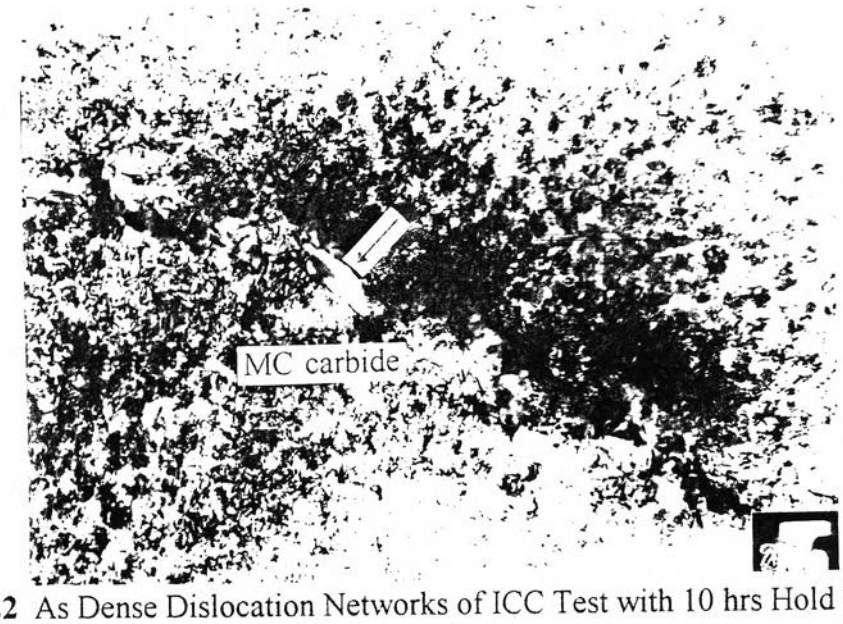

Figure 4.22 As Dense Dislocation Networks of ICC Test with 10 hrs Hold Time in TEM

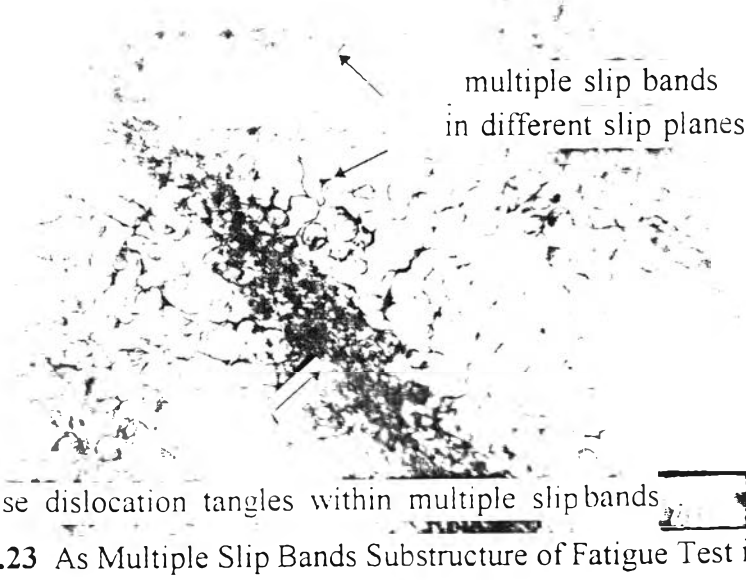

Figure 4.23 As Multiple Slip Bands Substructure of Fatigue Test in TEM

band acted as a barrier to movement of other dislocations. As results, it implied that the work hardening effect by the fatigue mechanism generated very lower strain when comparing to creep and isothermal cyclic creep tests.

However, in previous work **[10]**, it reported that the formation of planar slip bands was an evident that shearing precipitate particles must occur. In the present work, it was very difficult to distinguish that the shearing mechanism occurred within slip bands or not, probably because the shearing of precipitate particles was hidden from view by very dense dislocation tangles in slip bands of this investigated specimens. Assumption from previous work **[10]** reported that the shearing of precipitate particles by dislocation occurred early in the fatigue deformation process but was covered in the beginning cycles by the rapid hardening because the dislocation tangles blocked dislocation movement at slip band intersections.

4.5.2 Mechanical Properties of Isothermal Cyclic Creep Tests

The curves obtained from creep and isothermal cyclic creep tests in various holding times of 1, 3, 5 and 10 hrs. were shown in Diagram 4.2. Isothermal cyclic creep tests produced longer fracture life times than that of pure creep. This was due to the load relaxation. The fracture lifetimes corresponded to isothermal cyclic creep test were set in a sequence from maximum to minimum as 5, 3 which had life time value very close to that in 10 and 1 hr. holds, respectively as seen in Table 4.3.

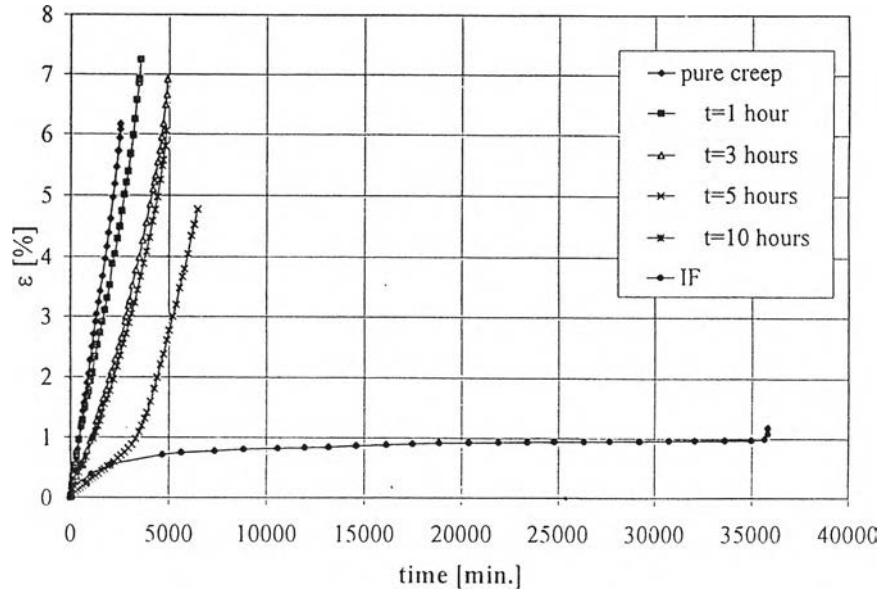

Diagram 4.2 Diagram of Strain-Time of ICC Tests

Holding Time (hrs.)	Fracture Strain (%)	Total Creep Life Time (min)	Number of Cycling (cyclic)	Cyclic Creep Strain Rate (mm/hr)
10	8.055	4,755	7	1.92×10^{-2}
5	6.578	6,055	20	5.997×10^{-3}
3	8.471	4,625	25	2.401×10^{-2}
1	9.064	3,406	57	4.314×10^{-2}

Table 4.3 Isothermal Cyclic Creep Tests Properties

The difference in strain rate of isothermal cyclic creep was also resulted from various holding times. All types of isothermal cyclic creep tests expressed lower strain rate than that of pure creep test, as shown in Table 4.3. The strain rates corresponded to isothermal cyclic creep tests were set in sequence from maximum to minimum as strain rate of 1 hr. holding time which was close to creep strain rate, 3 which had very similar value to that of 10 and 5 hrs. holds, respectively, as shown in Table 4.3. The extension of specimen guage length due to plastic deformation were measured after fracture. It can be also seen that the strains at fracture of all hold times and from pure creep were set in sequence from maximum to minimum as from 1, 3, 10, pure creep and 5 hrs. hold time respectively.

In case of 5 hrs. hold curve, it would be ignored due to the mistake of temperature controlling in the test although the temperature was set at 650°C from the begining of testing. There was temperature drop down unintendly from required constant temperature at 650°C in an interval after starting test. This produced the errors such as lower strain and strain rate. After this error range, temperature was adjusted to the given temperature again then curve with 5 hrs. hold increased highly again as seen in Diagram 4.2. Thus this obtained data from 5 hrs. hold test should not be considered or determined for further discussion.

Therefore, in case of the tests under holding times for 1, 3 and 10 hrs. holds, it can be shown that the time to fracture increased with increasing the duration of holding time but this phenomenon was contrast from previous studys **[7,10,12]**, they

were reported that fracture lifetime was inversely proportional with holding time duration. Therefore, by these obtained isothermal cyclic creep results and present information knowledge, it could not be made the conclusion. This might be an effect of very high values of tested maximum load (R_{max}=740 MPa) which was higher than yield strength (680 MPa) at 650°C. However, introduction of the additional cyclic loading component superimposed on the stationary creep resulted in an improvement of the fracture lifetime and decreasing in the cyclic creep strain rate in all isothermal cyclic creep tests comparing to that of pure creep.

4.6.1 Substructure Analysis of Cyclic Creep with TMF Tests

To study the substructure of specimens, thin foils were prepared and investigated in longitudinal sections of fractured specimens subjected to thermal and stress cycling in cyclic creep with TMF tests with 1 and 5 hrs. hold times. They showed that the substructure was very similar to those of all specimens under creep and isothermal cyclic creep tests. Very dense dislocation networks existed in matrix resulted from high deformation. The dislocation interactions with gamma prime particles were clearly observed in Figure 4.25. The Orowan bowing mechanism was occurred due to dislocations movement around particles and thus strengthened matrix.

In cyclic creep with TMF with 5 hrs. hold test, the substructure consisted of dislocation networks bowing precipitate particles and particles shearing. The main interaction with dislocation was Orowan bowing. When considering the results of

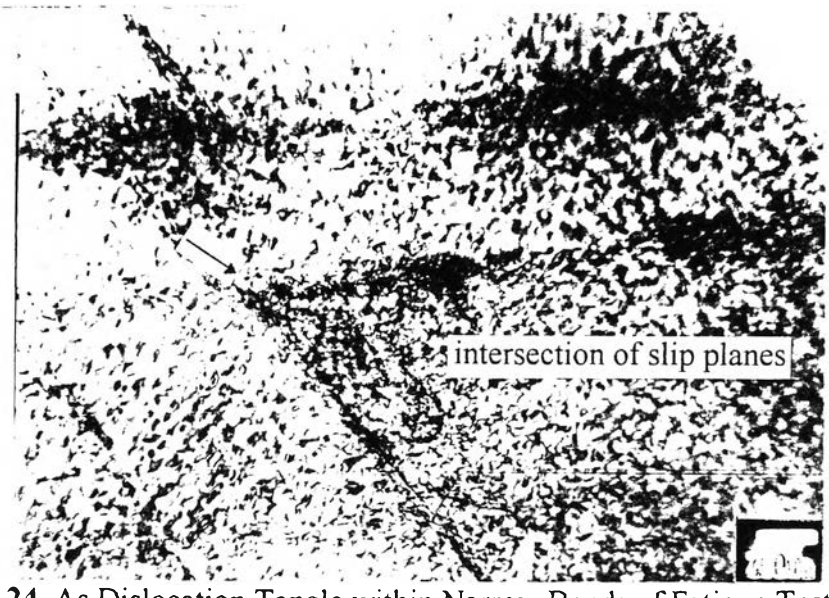

Figure 4.24 As Dislocation Tangle within Narrow Bands of Fatigue Test in TEM

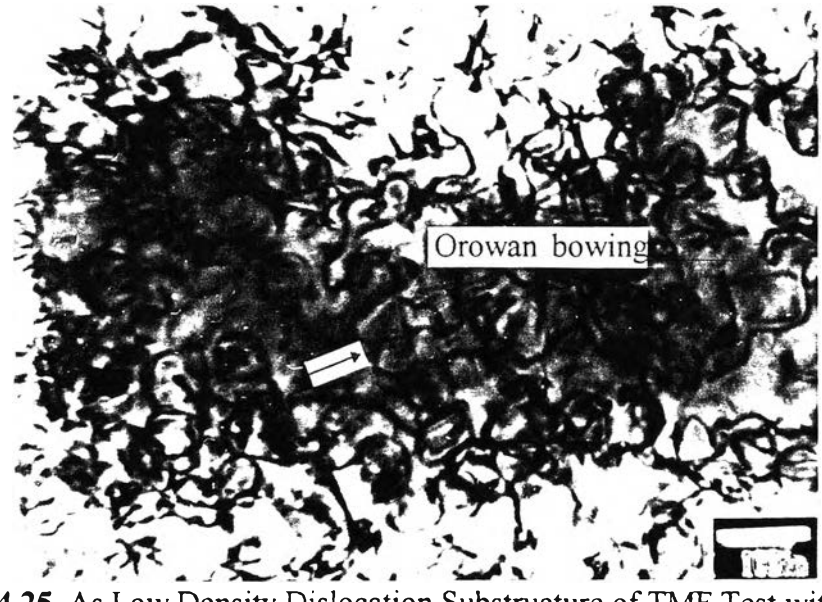

Figure 4.25 As Low Density Dislocation Substructure of TMF Test with 1 hr Hold Time in TEM

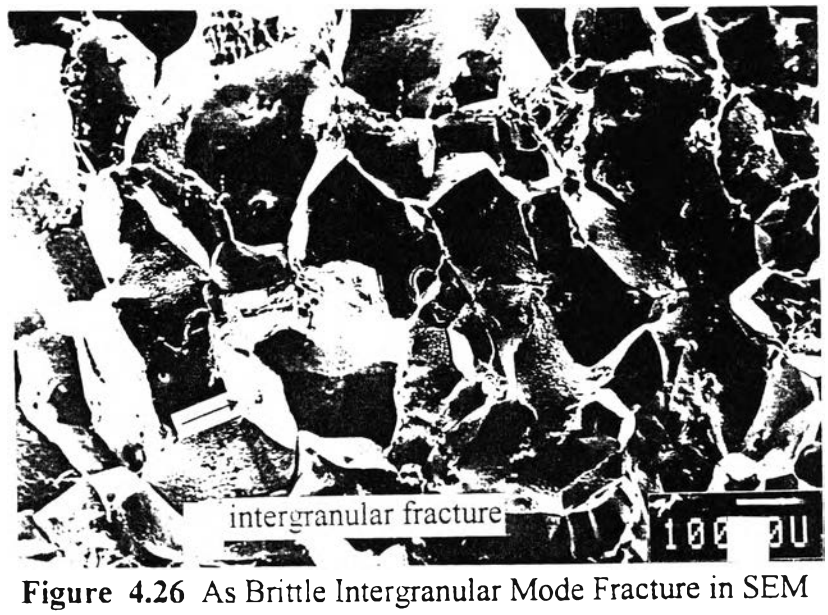

Figure 4.26 As Brittle Intergranular Mode Fracture in SEM

cyclic creep with TMF with 1 hr. hold test, there was no observation of particles shearing by dislocations. This would imply that shearing interaction occuring in primary creep intervals appeared at beginings of each cycle under cyclic creep with TMF test with 5 hrs. hold time may relate to higher strain rate than that in Orowan bowing interaction with dislocation of cyclic creep with TMF test with 1 hr. hold time.

4.6.2 Mechanical Properties of Cyclic Creep with TMF Tests

The temperature cycling and stress cycling were considered as factors to affect the creep process. This led to changes of fracture life, plastic behaviour and strain rate, as listed in Table 4.4. The experimental results of creep and cyclic creep with TMF testing are shown in Figure Diagram 4.3 and Table 4.4. All curves of cyclic creep with TMF data obtaining from individual testing also displayed longer fracture lifetime than that of pure creep.

However, in this TMF tests, all results which were obtained from TMF tests would be ignored due to the material mistake. From appendix page 97, the TMF tests diagram which also displays the amount of deformation including initial strains shows that these curves of all holding time tests did not run from the same point. This might be the effect of heterogenity of coarse block-like MC carbides which affected to mechanical properties of the alloy. Therefore, there will be no more for further analysis.

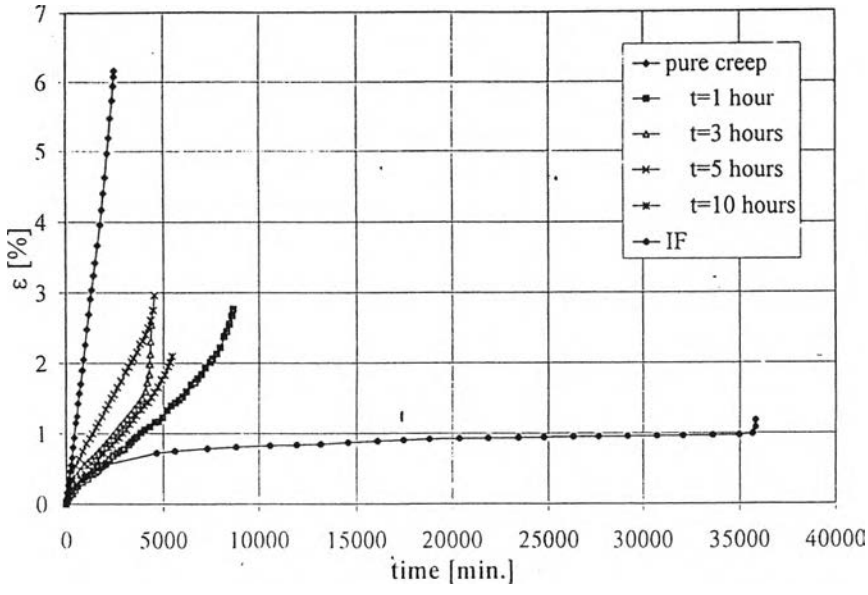

Diagram 4.3 Diagram of Strain-Time of TMF Tests

Holding Time (hrs.)	Fracture Strain (%)	Total Creep Life Time (min)	Number of Cycling (cyclic)	Cyclic Creep Strain Rate (mm/hr)
10	5.835	5,444	9	4.175×10^{-3}
5	6.247	4,402	14	6.352×10^{-3}
3	6.67	4,293	23	3.958×10^{-3}
1	4.78	7,910	131	2.364×10^{-3}

Table 4.4 Cyclic Creep with Thermomechanical Fatigue Stress Component tests properties

4.7 Fractography Analysis of Fractured Specimens

Metallographs of the fracture surface of the specimens of different creep stress levels, Isothermal cyclic creep and cyclic creep with TMF tests revealed in the similar manner that initiation of fracture crack was predominantly intergranular and these cracks nucleated on the free surface of specimens, as shown in Figure 4.26. This surface crack nucleation should occured either from grain boundary cavities and/or grain boundaries sliding. Subsequently, crack would propagated along grain boundaries in earlier stages of deformation process when the void spacing becomes small enough that voids can link up together.

Growth of this opening crack continued by intergranular propagating mode fracture. Only in surface regim around intergranular crack initiations, fracture surface oxidation was observed on all fractured specimens as an effect of surface oxidation formation which was exposed to hot air environment during cracks opening. However, this small area of surface oxidation insignificantly affected to fracture mechanism. In creep tests, the varying stress level did not show any significant difference in the mode of fracture when comparing to creep test exposed to 740 MPa.

However, all of isothermal cyclic creep fractured surfaces showed that the initial intergranular area fractions were lower than that of crept specimens. This was due to an effect of load relaxing. In this unloading duration, no stress assisted continuous dislocation movement to form cavities along grain boundaries. Thus the cavities could not agglomerate together to be intergranular fracture.

When initial crack reached a critical size, the propagation of crack under unstable condition continued by mixing mode presenting both intergranular and transgranular brittle clevage facets as the result of continuously increasing true stress in remaining cross section area of specimen, as shown in Figure 4.27. No harmfull oxidation was observed in mixing and transgranular ductile zones.

At the final state, transgranular ductile facets appeared dominantly on fracture surface, as illustrated in Figure 4.28. These transgranular ductile fracture facets were obtained during rapid crack growth as an effect of rapid reduction in cross section area. This transgranular ductile fracture mode might result from voids growth within grain, linking up of the voids occurred within grains, and subsequently generated dimple transgranular fracture. Thiese voids can be clearly seen in the regims arounded with coarse MC carbides due to high stress concentration.

However, no result of fatigue marks in isothermal cyclic creep tests were observed on the fracture surfaces for any holding time. This migth be the probable effect of unsufficient frequency of loading **[1]**. Thereafter, it could not generate fatigue damage mechanism. It also could be considered that creep accumulation was dominate mechanism for fracture under isothermal cyclic creep tests.

In case of pure fatigue at constant high temperature test, fracture mechanism was in transition stage **[1]** between low and high temperature behaviour which fracture

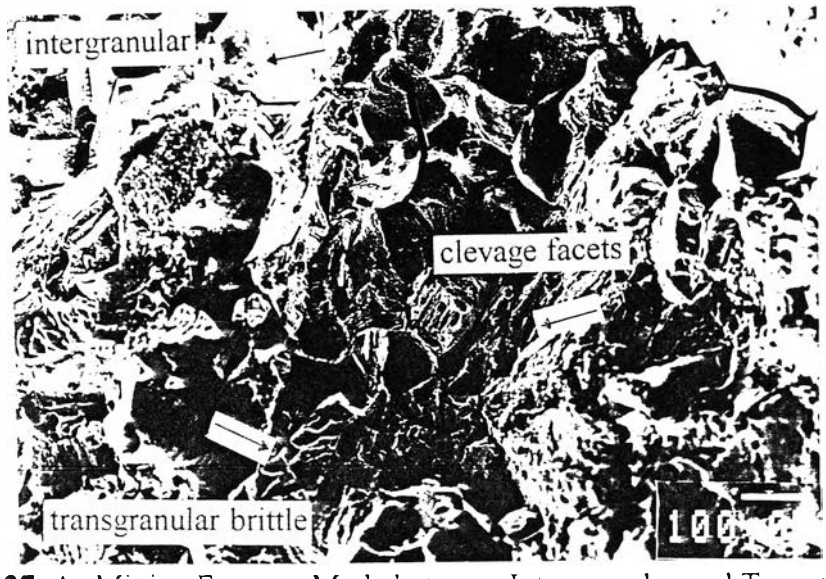

Figure 4.27 As Mixing Fracture Mode between Intergranular and Transgranular in SEM

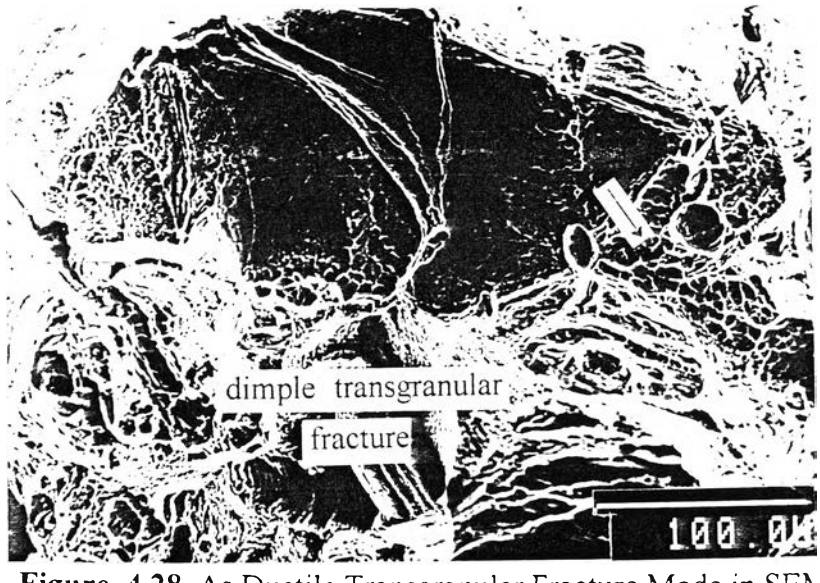

Figure 4.28 As Ductile Transgranular Fracture Mode in SEM

Figure 4.29 As Fracture Initiated Intergranularly from Fatigue Test in SEM

initiated intergranularly and then propagated primarily transgranularly, as illustrated in Figures 4.29 and 4.30. This fatigue fracture process might be the combination effects between increased stress concentration and strain rate at the crack tip.

At fatigue fracture initiation mechanisam of the alloy showed major characteristics as same as found in creep fracture mechanism. It can be explained that grain boundary sliding and/or cavitation was the principal mechanism in deformation. Crystallographic slip was more homogeneous and slip-band cracking was suppressed in favour of intergranular fracture **[1]**. Then crack propagation would take place. This can be divided into four stages according to previous theory **[1]**, as mentioned in literature survey, section 2.4.3.

In case of cyclic creep with TMF tests with 3, 5 and 10 hrs. holding times, any fatigue facet did not appear on initiation crack facet or in propagation stage of fracture crack. This was because either number of stress relaxing cycles or temperature cycling were not enough to support the fatigue stress component in fracture process. However, very small regim of fatigue facet at fracture surface was found for cycling test under 1 hr. hold time, as shown in Figure 4.31. This might be the result of high number of loading cyclic provided enough slip plains to generate small fatigue facet at fracture surface.

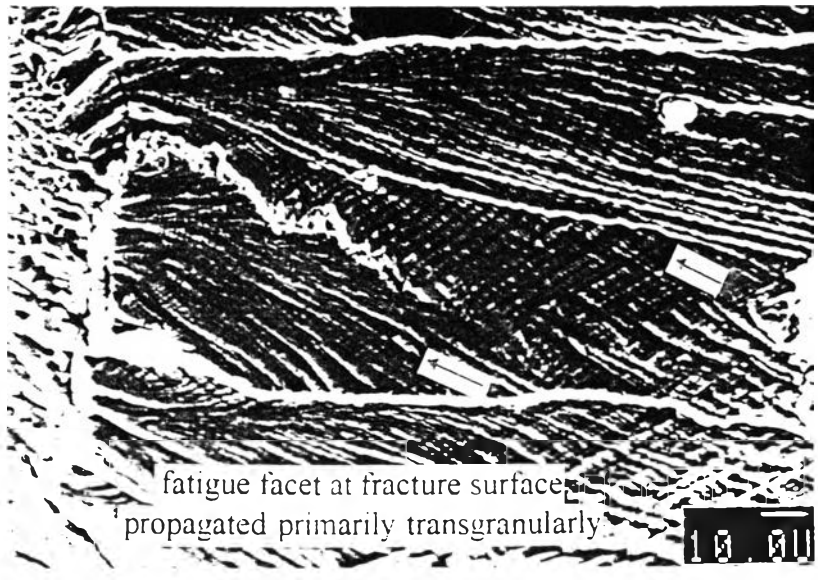

Figure 4.30 As Fracture Propagated Transgranularly from Fatigue Test in SEM

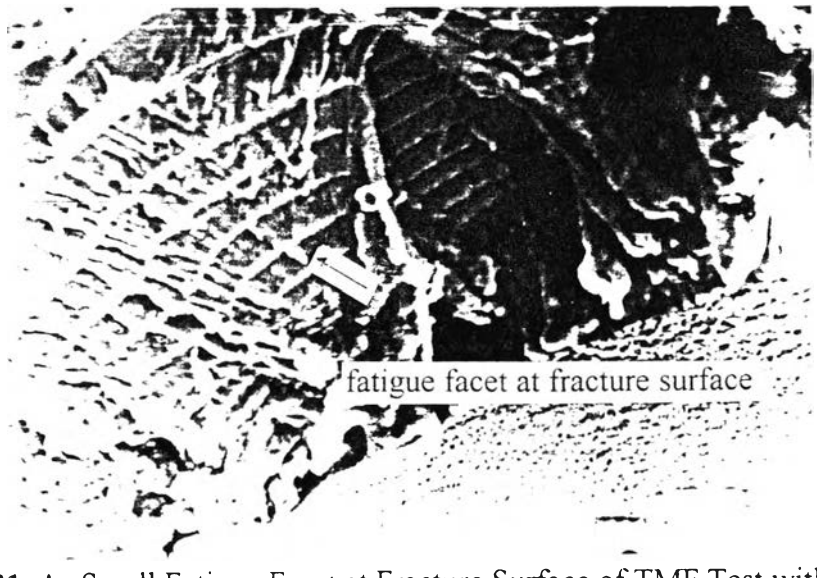

Figure 4.31 As Small Fatigue Facet at Fracture Surface of TMF Test with 1 hr Hold Time in SEM